Scientific Research Publishing

Open Journal of Geology, 2022, 12, 234-249
https://www.scirp.org/journal/ojg
ISSN Online: 2161-7589
ISSN Print: 2161-7570

Research on Surrounding Rock Stability Test of Tunneling Roadway under Complex Geological Conditions

Maoru Fu[1], Binyang Sun[1], Liquan Guo[1*], Zan Ye[2], Xiangxiang Zhuang[2]

[1]School of Earth and Environment, Anhui University of Science and Technology, Huainan, China
[2]Coal Industry Branch of Huaihe Energy Group, Paner Coal Mine, Huainan, China
Email: *guoliquan78@126.com

How to cite this paper: Fu, M.R., Sun, B.Y., Guo, L.Q., Ye, Z. and Zhuang, X.X. (2022) Research on Surrounding Rock Stability Test of Tunneling Roadway under Complex Geological Conditions. *Open Journal of Geology*, **12**, 234-249.
https://doi.org/10.4236/ojg.2022.123013

Received: February 22, 2022
Accepted: March 14, 2022
Published: March 17, 2022

Abstract

Different geological conditions are often encountered in the excavation of coal mine roadways, with fault-fracture zone being the most commonly seen complex geological conditions. Fault-fracture zone is characterized by complex lithologic property and joint development and can easily cause safety accidents when excavation burrows through the fault. Therefore, grouting reinforcement of fault-fracture zone is often implemented to ensure coal mine safety production. Based on the tunnel excavation case of −530 - −650 m belt conveyor inclined roadway at Huainan Pan'er Coal Mine, borehole optical fiber and electrical testing technologies were applied to monitor and analyze the dynamics of the surrounding rock stability when roadway excavation passed through the F1 fault, and evaluate the effect of grouting reinforcement on fault-fracture zone. According to the results of optical fiber and electrical methods, the distributional characteristics and evolution patterns of strain and electric resistivity were analyzed. The research pointed out the distinct difference in variation characteristics of strain and electrical fields between grouted reinforced fault-fracture zone and normal rock strata sections. This indicates that the grouting reinforcement effectively improve physical properties of rock strata in the fractured section, the stability of the rock strata at the fault-fracture zone was effectively increased, the degree of fault activation and deformation was relatively small, and roadway surrounding rock basically retained its original properties, pointing to high stability.

Keywords

Fault-Fracture Zone, Activation, Dynamic Monitoring, Stability

1. Introduction

A variety of geological problems are often encountered when underground roadway excavation is carried out in coal mine. These geological problems are usually attributable to changes in geological conditions, such as fault zone, collapse column and seam thinning zone. These geological conditions are complex for normal sedimentary strata and can cause accidents like water inrush and collapse of roof rock, thus affecting coal mine safe production. Specifically, fault-fracture zone is one of the most commonly seen complex geological conditions. Subject to the effect of mining activities in the coal-bearing strata, the fault-fracture zone is often activated, causing geological disasters like water inrush, pressure bump and coal and gas outbursts [1]. Therefore, researching the testing technology of surrounding-rock stability in roadway excavation under complex geological conditions is of great significance for guiding safe production of coal enterprises.

Presently, extensive scholarly research and analyses on stability control technology in roadway excavation at faults and fractured rock mass have been conducted with good outcomes. Zhang Jinggong proposed that applying combined forepoling technology in fault construction can effectively control surrounding rock deformation, increase safety and reliability of construction and provide approaches and referenceable experience for handling problems like roof caving [2]. Through an analysis of fault occurrence and throw, Shi Zhiyin proposed measures like horizon control and laying metal mesh on fault-fracture zone to ensure safet production on the fully mechanized caving face [3]. Utilizing grouting reinforcement measures such as Gutelong (GN-4 model), Zhou Qinglin *et al.* effectively solved the geological degree of fracture development and increased the stability of surrounding rock [4]. Based on an analysis of the mechanism of grouting of fractured rock mass caving, Zhang Yong proposed the advanced deep-borehole grouting reinforcement technology to prevent roof caving of fault-fracture zone, which yielded good results in practice [5].

As can be seen from above, present scholarly research has focused on controlling stability of fault-fracture zone through integrated measures like advanced borehole grouting and pre-support, however, few studies have addressed stability analysis of the rock mass of fault-fracture zone after grouting reinforcement [6] [7] [8] [9]. More scholarly attention should be focused on what methods should be adopted to evaluate the stability characteristics of rock mass in fault-fracture zone after grouting treatment. On that basis, this paper presents a study of the F1 fault zone passed through the −530 - −650 m belt conveyor inclined roadway at Huainan Pan'er Coal Mine. Integrated measures encompassing the borehole distributed optical fiber sensing and electrical method were mainly applied to conduct full-cycle dynamic monitoring, which derived stability conditions of the fracture zone after receiving grouting reinforcement treatment, followed by an evaluation of the stability of the zone. Through this study, the reliability of the relevant methods is tested, and the stability characteristics of F1 fault are obtained, which can effectively guide the safe production of the mine.

2. Project Overview

The F1 fault zone is abounding fault between Panbei and Pan'er mining areas, with a fault throw of 10 - 300 m. The Panbei and Pan'er coal mining areas were required to be merged for purpose of resource integration. The merging was fulfilled by an inclined roadway connecting the two coal mining areas using the −530 - −650 m belt conveyor inclined roadway, which would pass through the F1 fault zone during excavation process, as shown in **Figure 1**. An investigation reveals that the F1 fault zone involved massive rock core fracture, obvious mudstone kneading and a large number of cracks with regional cracks being filled with calcite vein. The fault-fracture zone was characterized by a great thickness, developing fault zone and subjection to great compressional stress. Rock in the fractured zone had a moderate degree of cementation, and on both sides of the fault were largely soft rock. Given the complex geological conditions of the F1 fault zone such as large fault throw and high fracture degree in the fractured zone, as well as redistribution of stress in surrounding rock masses caused by roadway excavation, considerably large safety hazard was expected to be encountered when the −530 - −650 m belt conveyor inclined roadway was excavated. As such, grouting reinforcement of the F1 fault zone had been conducted from ground surface in the initial stage.

To evaluate the effect of ground grouting treatment of the F1 fault zone passed through the −530 - −650 m belt conveyor inclined roadway and analyze the stability of surrounding rock of the roadway section, distributed optical fiber sensing technology and parallel electrical method were adopted in the integrated monitoring project of the F1 fault zone.

3. Principles of Monitoring Methods

3.1. Optical Fiber Sensing

The Brillouin optical time domain reflectometry (BOTDR)-based distributed optical fiber sensing technology was adopted in monitoring. By principle, after the pulsed light emitted by the demodulator is injected into the optical fiber, the photons and phonons in the optical fiber experience elastic and inelastic collisions and Brillouin scattering will be generated along the opposite direction to the transmission of the pulsed light. Brillouin scattering light is sensitive to both strain and temperature in the testing environment. When change in strain or temperature of a certain point occurs, the Brillouin frequency shift of the point will occur. Changes in strain and temperature can be obtained based on the change in Brillouin frequency shift. The relationship between Brillouin frequency shift and the two factors can be expressed by Equation (1).

$$\nu_B(\varepsilon,T)=\nu_B(0)+C_\varepsilon\cdot\varepsilon+C_T\cdot T \tag{1}$$

where $\nu_B(\varepsilon,T)$ is the Brillouin frequency shift under the dual effects of strain and temperature; $\nu_B(0)$ is the Brillouin frequency shift in the initial state; C_ε is the strain coefficient of Brillouin frequency shift, 0.05 MHz/με; C_T is the temperature coefficient of Brillouin frequency shift, 1.1 MHz/με.

3.2. Electrical Resistivity Testing

With respect to the electrical resistivity method in boreholes, the parallel electrical testing system was applied. Based on the working principle of high-density resistivity method, the testing system adopts the "distributed parallel intelligent electrode potential difference signal acquisition method and system" to collect and interpret data. The biggest advantage of the testing technology lies in the fact that when any electrode deployed in the system is supplied with electricity, potential measurement can be simultaneously conducted at all of the rest electrodes, allowing for a clear reflection of changes in spontaneous potential in detected area and in potential of the primary field potential of electricity supply and significantly higher data collection efficiency compared with traditional high density resistivity method [10]. Depending on the field source of electricity supply point, data collection of the parallel electrical testing system can be divided into the AM and ABM methods. A large body of electrical data can be obtained by automatic sequential switch of electrodes implemented by the AM and ABM-based devices, which not only fulfill data inversion of all existing DC-high density resistivity methods (e.g., Zener diode, triode and tetrode) and high-resolution inversion by resistivity method [11]-[16]. In AM method, wenner tripole method is used for electrical data acquisition, and in ABM method, Wenner quadrupole method is used for electrical data acquisition.

4. Monitoring Scheme

4.1. Deployment of Monitoring Borehole

Based on the investigation tasks and actual conditions, a borehole monitoring system encompassing devices based on the BOTDR and electrical methods was deployed in −530 - −650 m belt conveyor inclined roadway. The monitored cross section was located near the 38 m ahead of the PD77 point in the inclined roadway excavated by the belt conveyor, and the testing systems were respectively installed on both sides of the roadway from the drilling field. The boreholes are shown in **Figure 1**. When testing was conducted, monitoring sites were deployed on the cross section to research the effect of inclined roadway excavated by belt conveyor on the rock strata of the F1 fault zone. As shown in **Figure 1(b)**, the 4 boreholes on the two cross sections were deployed at a certain depth of the F1 fault-fracture zone. As such, the boreholes at 4 different directions formed up a 3-dimensional monitoring space capable of robustly evaluating the structural stability of the F1 fault-fracture zone near the same section of inclined roadway excavated by the belt conveyor.

4.2. Data Collection and Analysis

On-site coal mine data collection started on March 26, 2020. Depending on the speed of roadway excavation and schedule of the mine owner, the frequency of data collection slightly varied. In the early stage, data collection frequency was once every 3-4 days; the construction of inclined roadway by the belt conveyor

was completed on May 20. From the date of construction completion to June 22, the frequency of data collection was still once every 3-4 days; after the data was stabilized, data collection frequency was changed to once every 15 days. The speed of excavating in the belt conveyor inclined roadway and part of the collection cycles are shown in **Table 1**. The excavation face of the inclined roadway by

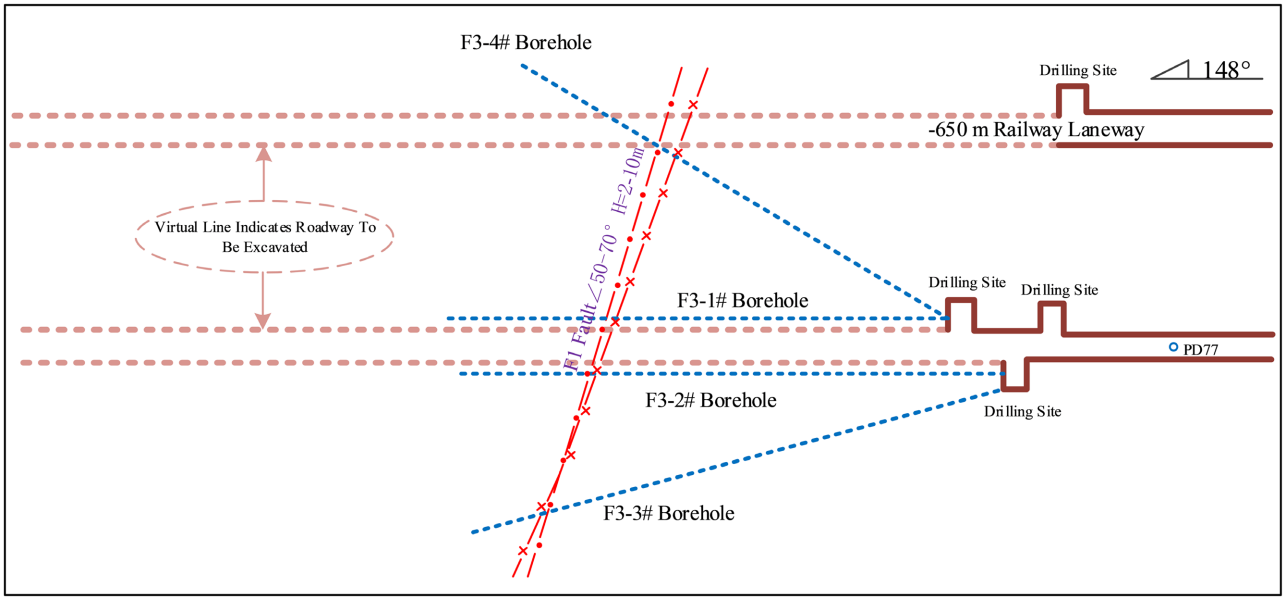

(a)

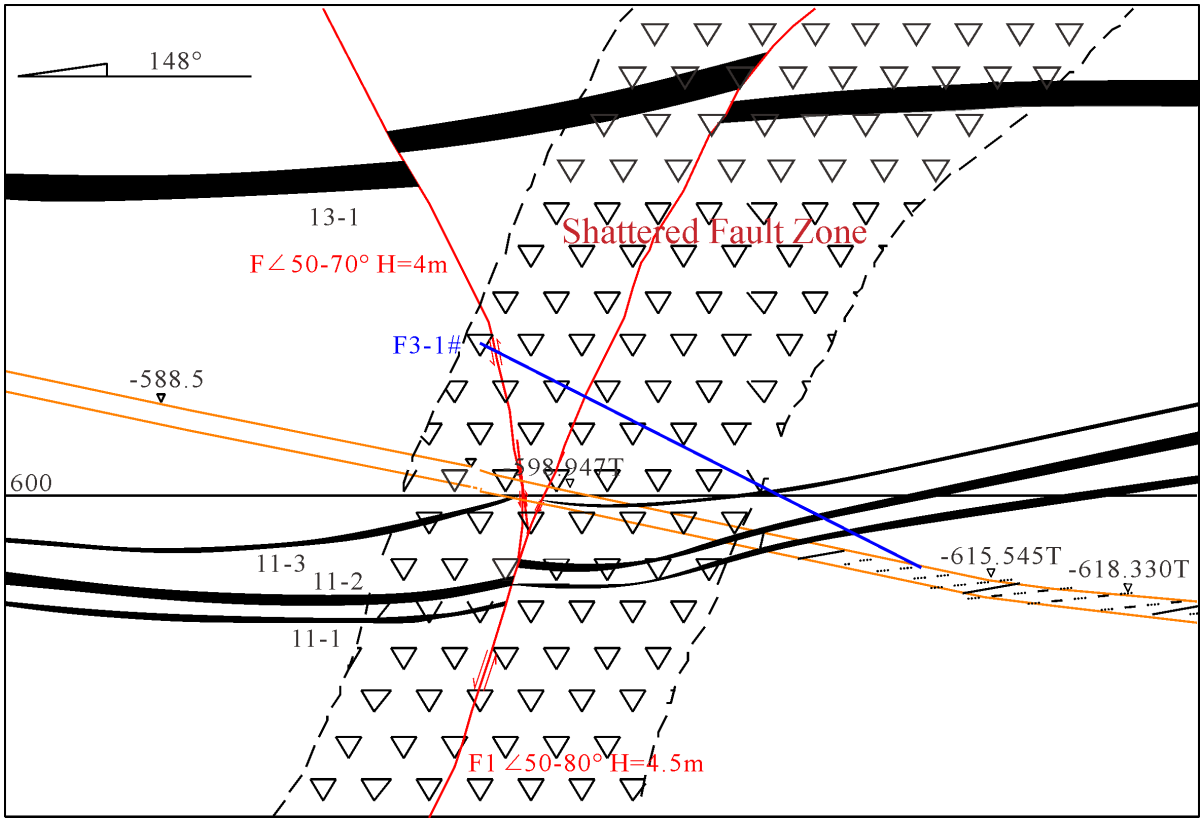

(b)

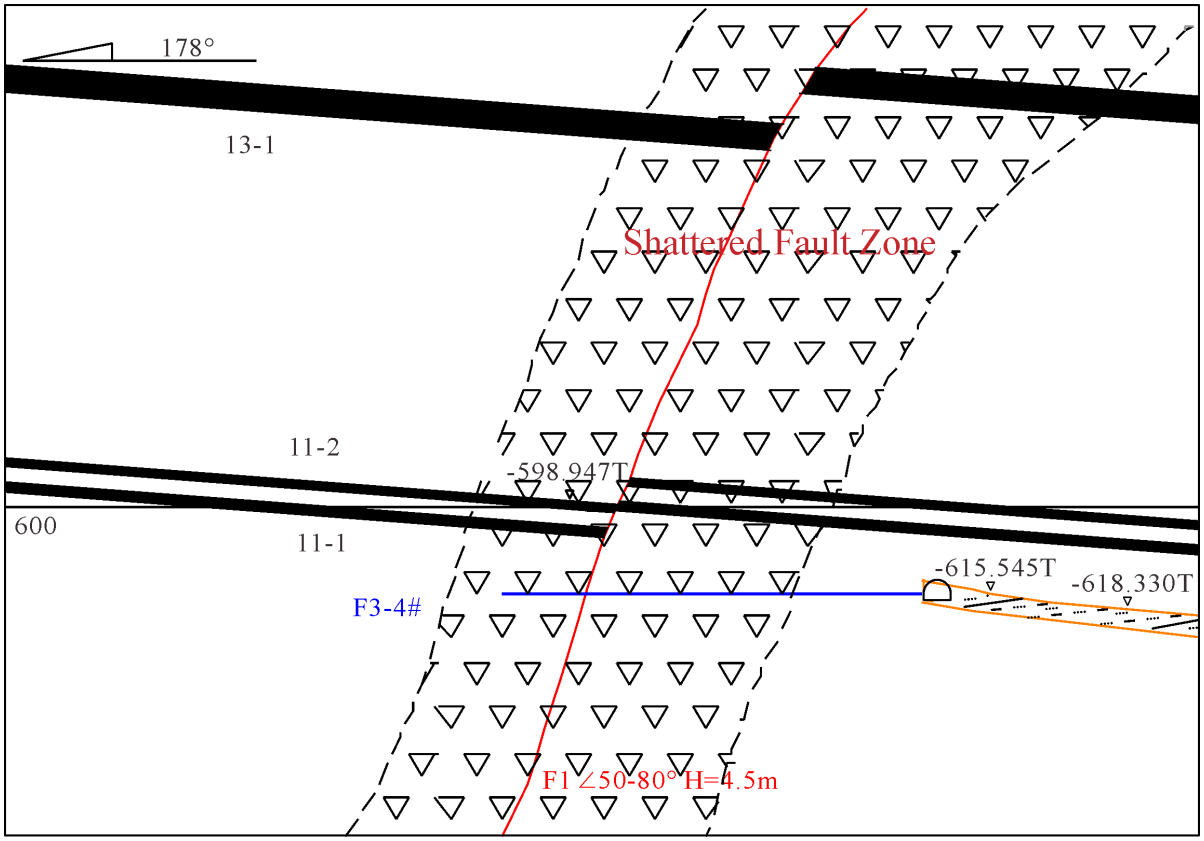
178°
13-1
Shattered Fault Zone
11-2
-598.947T
600
11-1
-615.545T
-618.330T
F3-4#
F1∠50-80° H=4.5m

(c)

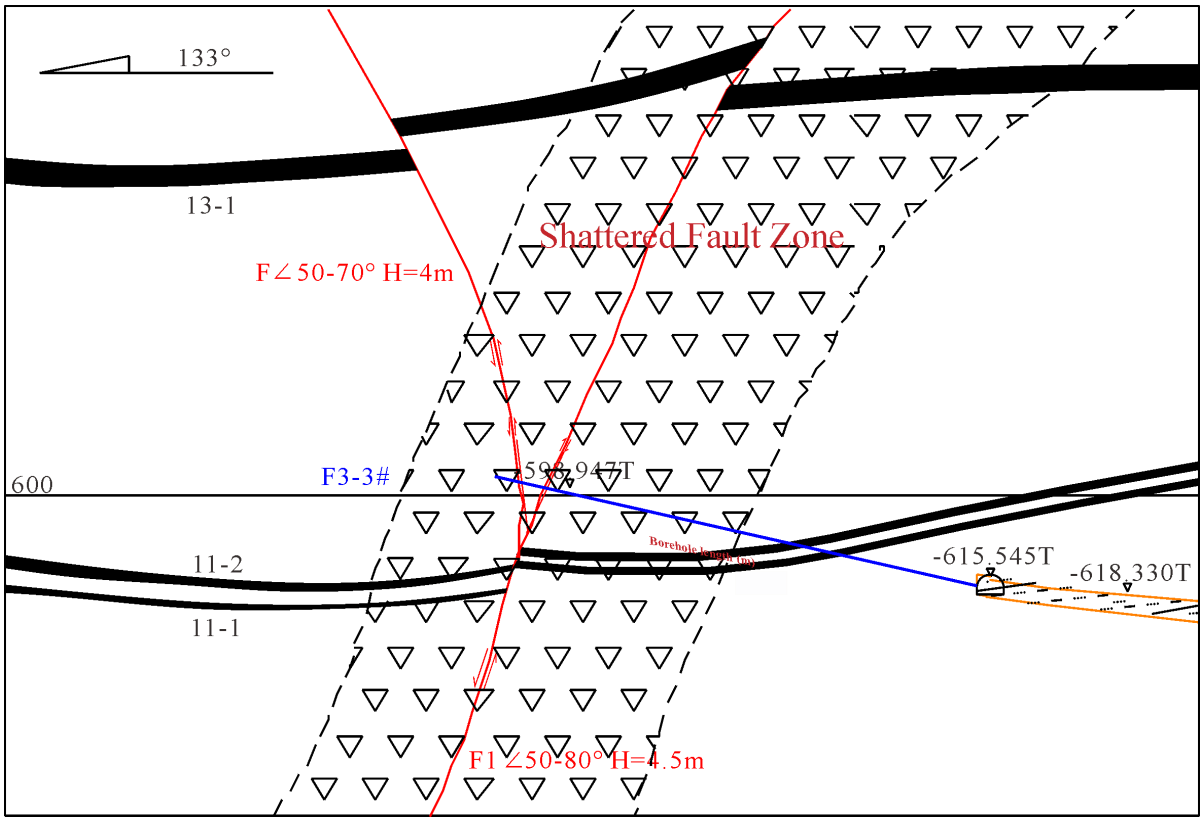
133°
13-1
Shattered Fault Zone
F∠50-70° H=4m
600
F3-3#
-598.947T
11-2
-615.545T
-618.330T
11-1
F1∠50-80° H=4.5m

(d)

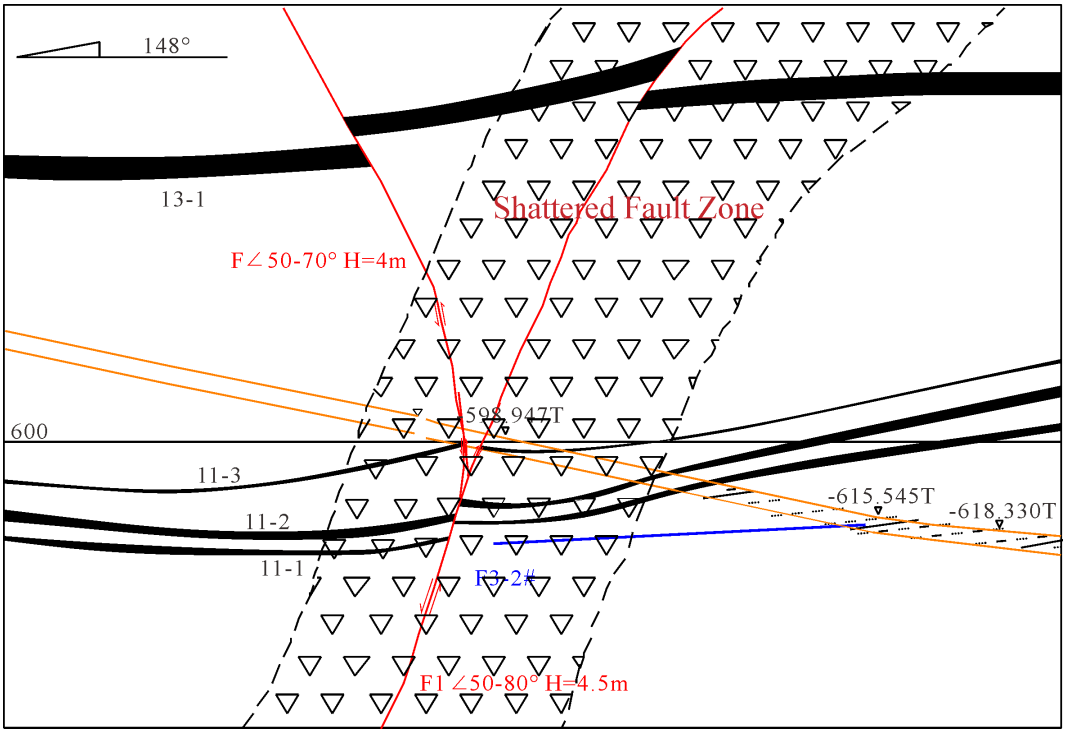

(e)

Figure 1. Schematic diagram of F1 fault monitoring borehole in −530 - −650 m belt conveyor inclined roadway. (a) Plane position map of monitoring hole; (b) Location map of F3-1 monitoring hole; (c) Location map of F3-4 monitoring hole; (d) Location map of F3-3 monitoring hole; (e) Location map of F3-2 monitoring hole.

Table 1. Roadway head-on position and partial monitoring cycle.

serial number	monitoring period	roadway head-on position (m)	Distance from fault zone(m)
1	20200326	PD78 + 25	22 m outside the fault
2	20200403	PD78 + 32.8	14 m outside the fault
3	20200405	PD78 + 35.2	11 m outside the fault
4	20200408	PD78 + 37.7	9.3 m outside the fault
5	20200412	PD78 + 43.7	3.3 m outside the fault
6	20200415	PD78 + 46.3	0.7 m outside the fault
7	20200417	PD78 + 47.5	0.5 m in the fault
8	20200420	PD78 + 51.1	4.1 m in the fault
9	20200423	PD78 + 54.7	7.7 m in the fault
10	20200427	PD79 + 21.1	17.1 m in the fault
11	20200430	PD79 + 23.5	19.5 m in the fault
12	20200502	PD79 + 25.3	21.3 m in the fault
13	20200505	PD79 + 30.1	26.1 m in the fault
14	20200508	PD79 + 34.9	30.9 m in the fault

Continued

15	20200512	PD79 + 43.5	39.5 m in the fault
16	20200516	PD80 + 11.6	44.6 m in the fault
17	20200519	PD80 + 16.7	49.7 m in the fault
18	20200520	Excavation completed	49.7 m in the fault
19	2020-6-1	Excavation completed	49.7 m in the fault
20	2020-6-22	Excavation completed	49.7 m in the fault
21	2020-8-20	Excavation completed	49.7 m in the fault
22	2021-1-22	Excavation completed	49.7 m in the fault

the belt conveyor was located at PD78 + 25 m, where data was collected for the first time as background values. As excavation of the inclined roadway went on, full-cycle strain and electric fields data range from the background data prior to the influence of inclined roadway excavation, the fault influenced by the roadway passing through the fault, the formation of deformation, to stabilized rock strata after roadway penetration. In the meantime, there were few data outliers for the BOTDR and electrical methods and data quality was generally high, ensuring the scientificness and reliableness of the data.

5. Monitoring Data Analysis

5.1. Analysis of Strain Field Data

Given limited length of this paper, data of F3-3# borehole was focused despite a large body of monitoring data collected from the test site. From April 17, 2020 to August 21, 2021, a total of 95 groups of strain deformation data by the BOTDR method were collected. Based on the analysis of the results of the BOTDR tests at different depths of the monitoring borehole, the observational data of surrounding rock deformation within the control range of the borehole in the monitoring cycle was obtained. On that basis, the stability of rock in F1 fault within the control range of the borehole was analyzed, followed by an evaluation of the grouting reinforcement from ground surface and monitoring of the stability of surrounding rock in the F1 fault during roadway construction and post-construction utilization stage. **Figure 2** shows the strain distribution based on the BOTDR method in the F3-3# borehole during the monitoring period. As can be seen, BOTDR-measured strain exhibited different strain characteristics, including both tensile and compressive strain, for different locations of borehole during the monitoring periods. The compressive strain was dominant and had relatively small amplitudes with the largest strain not exceeding 600 $\mu\varepsilon$, indicating a small rock strata deformation within the control range of the borehole and relative stability in fault-fracture zone.

To better analyze deformation and damage of rock strata within the control range of borehole, the strain curve and geological profile were combined to comprehensively analyze rock strata deformation, as shown in **Figure 3**. The

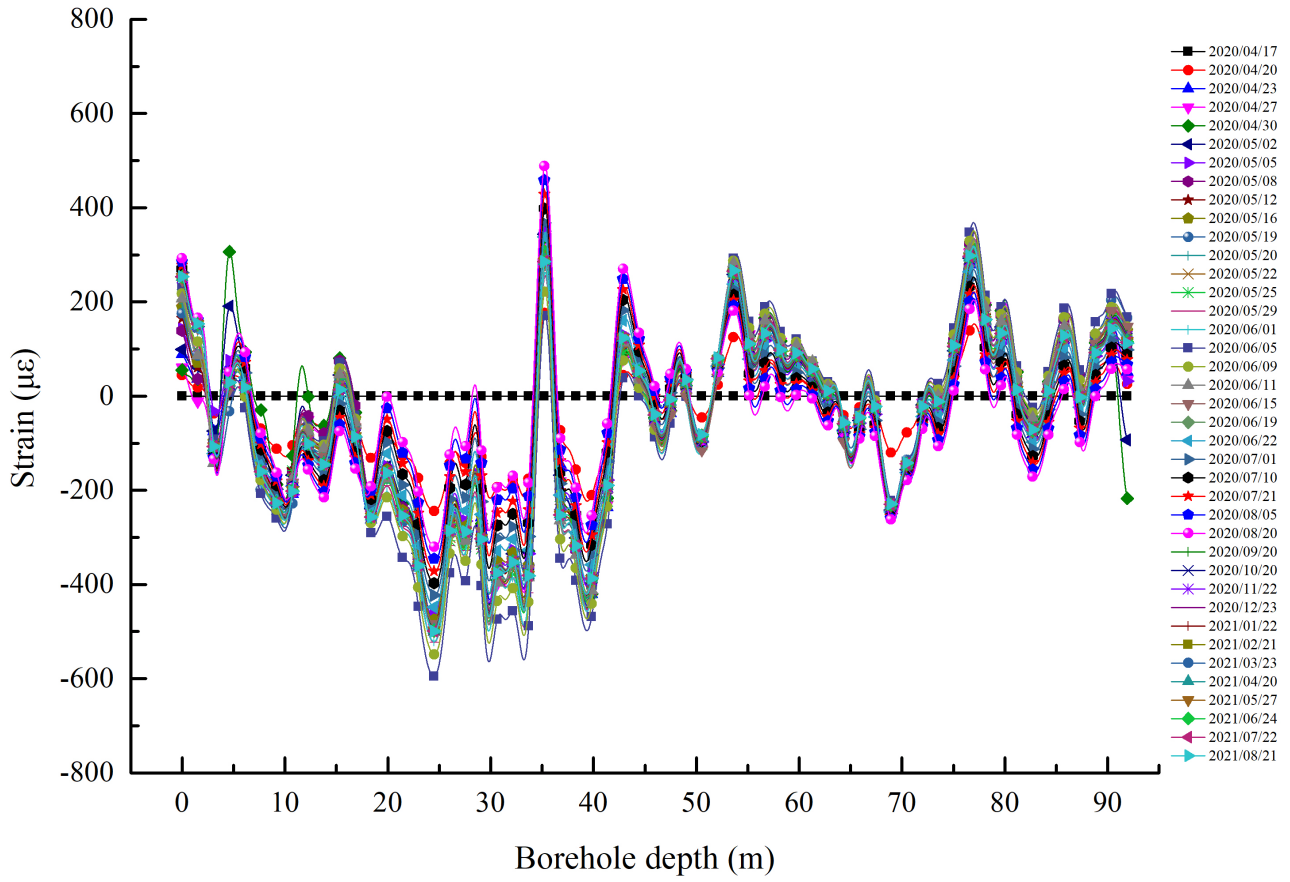

Figure 2. Strain distribution of F3-3# borehole

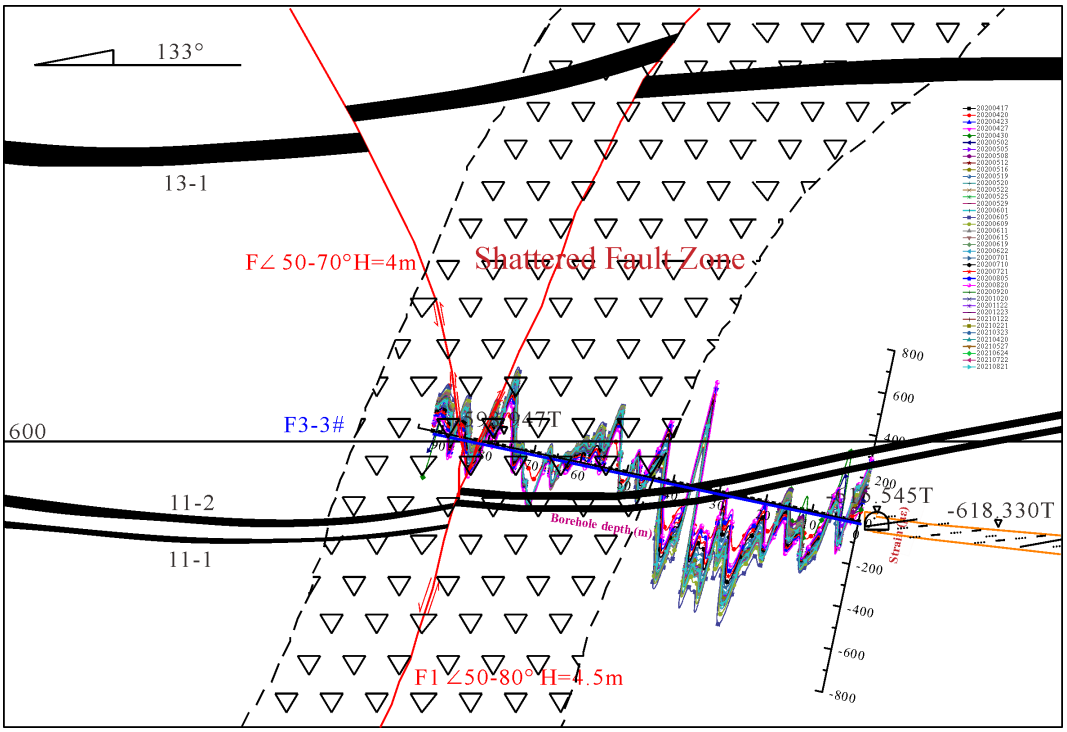

Figure 3. Strain curve change of rock stratum in F3-3# borehole.

control range of borehold mainly encompassed two geological bodies: First, the F1 fault-fracture zone; second, the normal lithologies like coal seams and sandy mudstone. Distinct difference in strain changes of the two geological bodies was observed. Specifically, grouting reinforcement of the F1 fault-fracture zone changed the original properties of fractured rock strata, which were dominated by concrete blocks with significantly increased elasticity modulus. Thus, the magnitude of strain change was relatively small compared with coal seam and sandy mudstone with normal lithology. This indicates that the integrity of rock strata in F1 fault-fracture zone was improved by grouting reinforcement from ground surface, and the mechanical properties of rock, including compressive and tensile strengths, were significantly increased.

As can be seen from **Figure 3**, there was a significant difference in strain changes between areas of normal lithology and fault-fracture zone. Prior to roadway penetration, the strain within the range of the fault-fracture zone controlled by the F3-3 borehole was dominated by tensile strain, and extreme values of tensile and compressive strengths in borehole appeared in certain periods before roadway penetration. However, with roadway excavation and its subsequent operation upon completion, the BOTDR-measured strain within the control range of the borehole was in a stable state. This indicates that in the roadway operation stage, the activation degree of the F1 fault-fracture zone was low and basically stabilized.

5.2. Analysis of Geoelectrical Field Data

The data generated by the underground electrical method was collected between March 26, 2020 to August 21, 2021; a total of 298 groups of data were collected. Based on the distribution characteristics of electrical parameters of the investigated cross section, the patterns of rock strata deformation and damage in the fault were examined. On that basis, rock stability of F1 fault-fracture zone within the control range of borehole was analyzed, followed by an evaluation of the effect of grouting from ground surface and monitoring of the stability of the surrounding rock of F1 fault during the construction and operation stages of the roadway.

Figure 4(a) presents the results of apparent resistivity of the surrounding rock within the control range of the F3-3 borehole collected on March 26, 2020. The investigation results were used as the background results of the borehole to be compared with subsequent test results, and on that basis, the variation patterns and characteristics of the fault rock strata within the control range of borehole were analyzed. As can be seen from the figure, the overall apparent resistivity was stable and fell in the 80 - 180 Ω·m range, indicating that the surrounding rock within the control range of the borehole had a relatively good structure and integrity, and the overall apparent resistivity values should reflect performances of normal sand, mudstone strata and silty sandstone without being significantly influenced by concrete grout. In general, the rock strata had a relatively poor

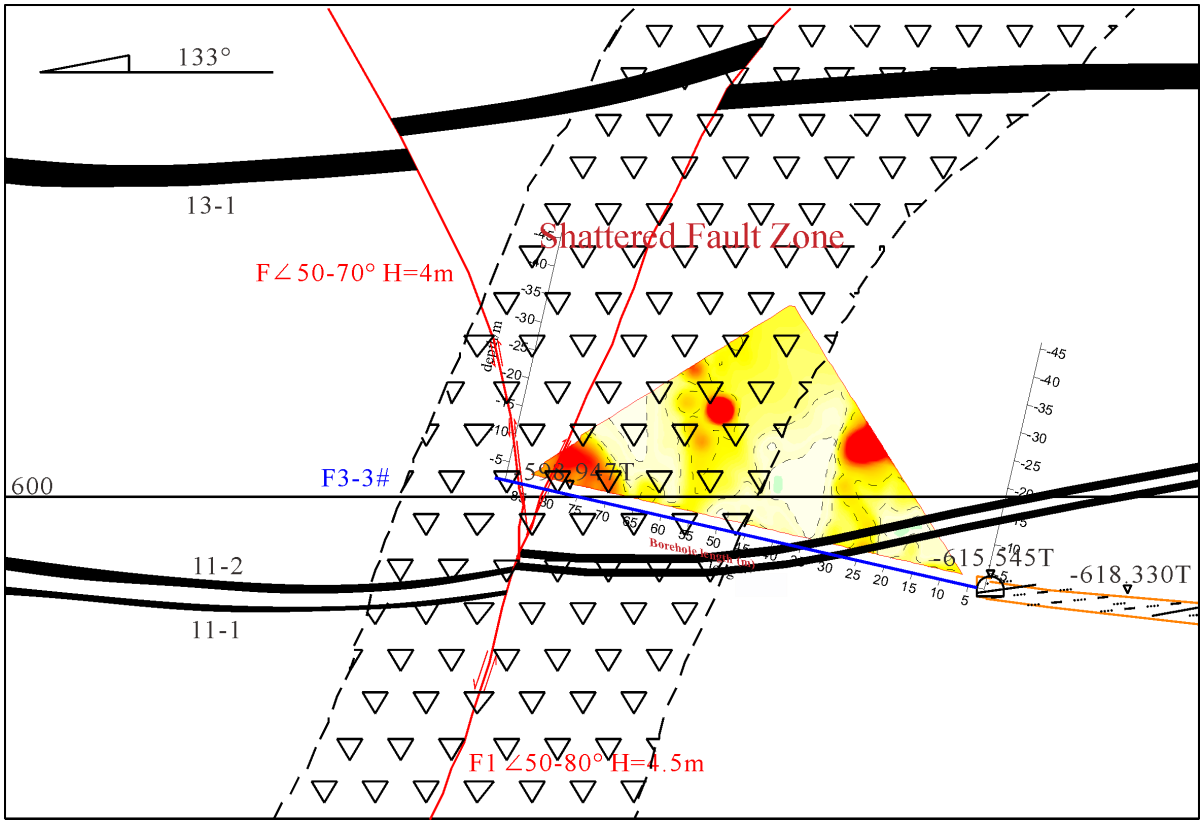
133°
13-1
Shattered Fault Zone
F∠50-70° H=4m
600
F3-3#
-598.947T
-615.545T
-618.330T
11-2
11-1
F1∠50-80° H=4.5m

(a)

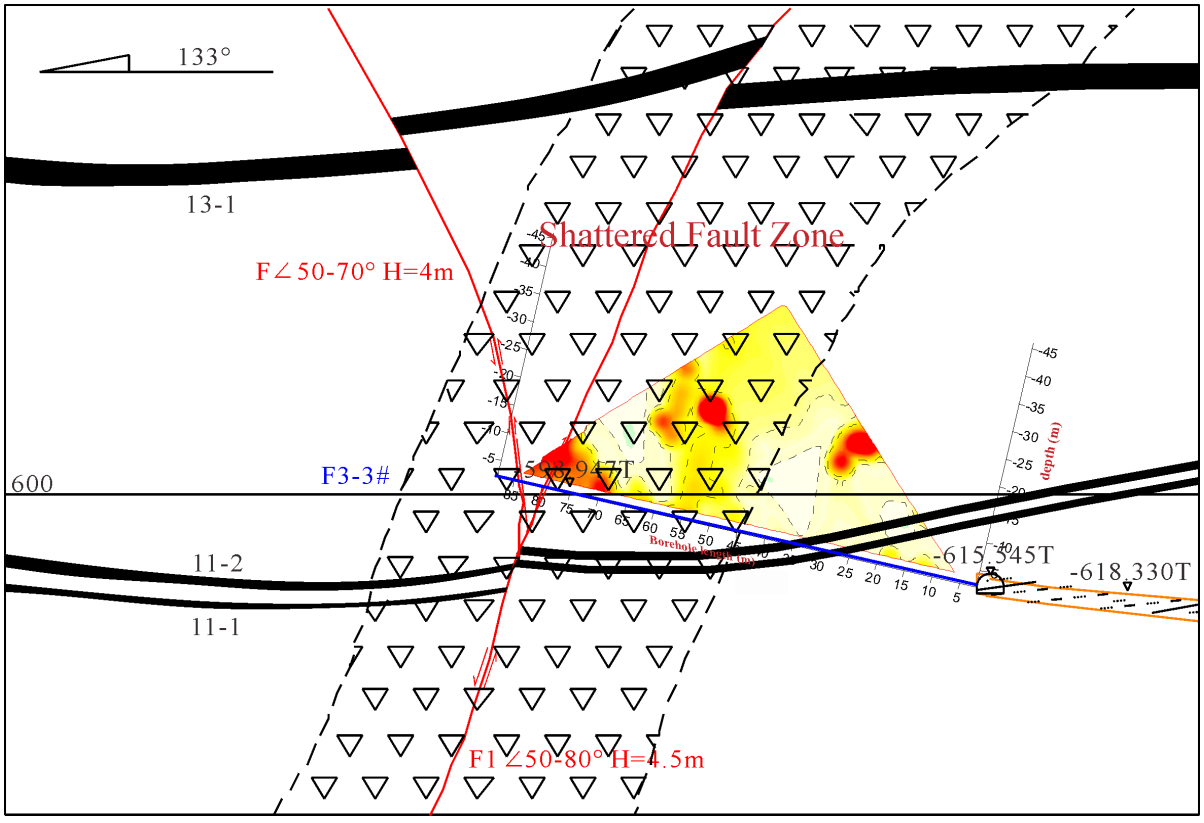
133°
13-1
Shattered Fault Zone
F∠50-70° H=4m
600
F3-3#
-598.947T
-615.545T
-618.330T
11-2
11-1
F1∠50-80° H=4.5m

(b)

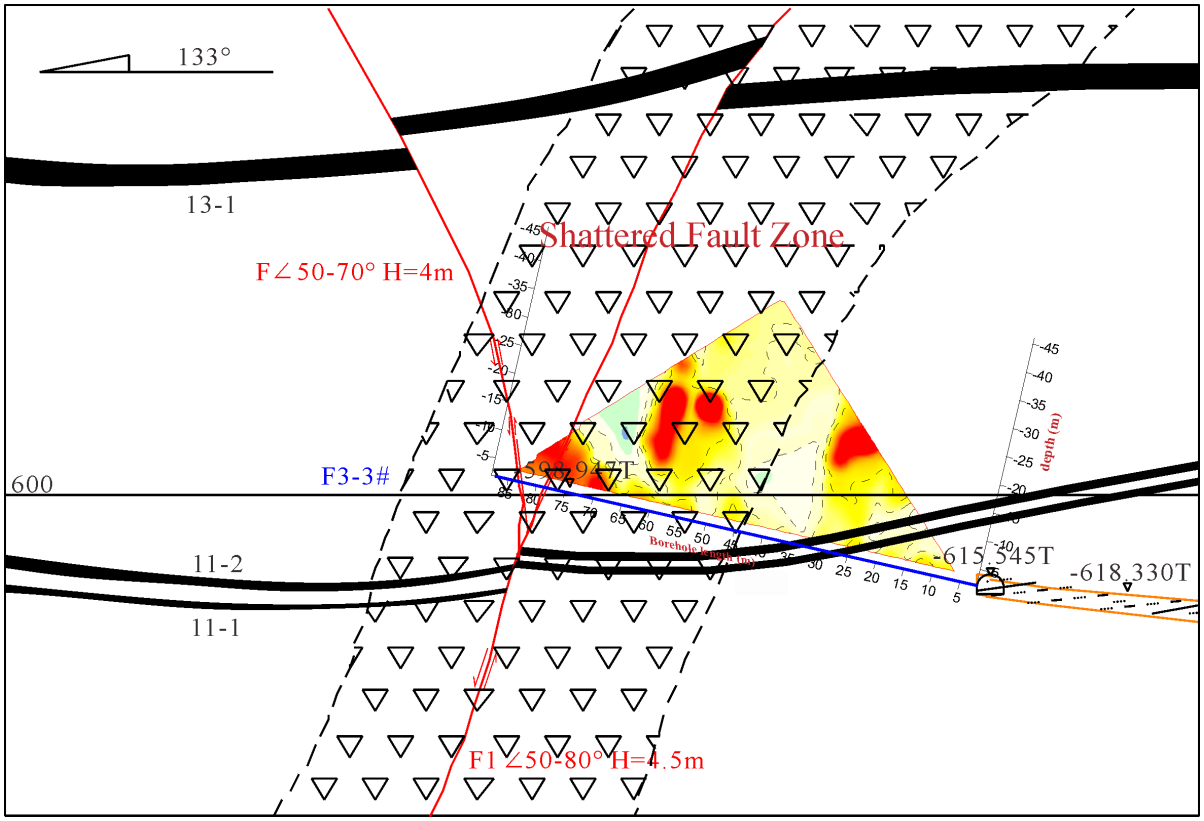
133°
13-1
Shattered Fault Zone
F∠50-70° H=4m
F3-3#
600
11-2
11-1
-615.545T
-618.330T
F1∠50-80° H=4.5m

(c)

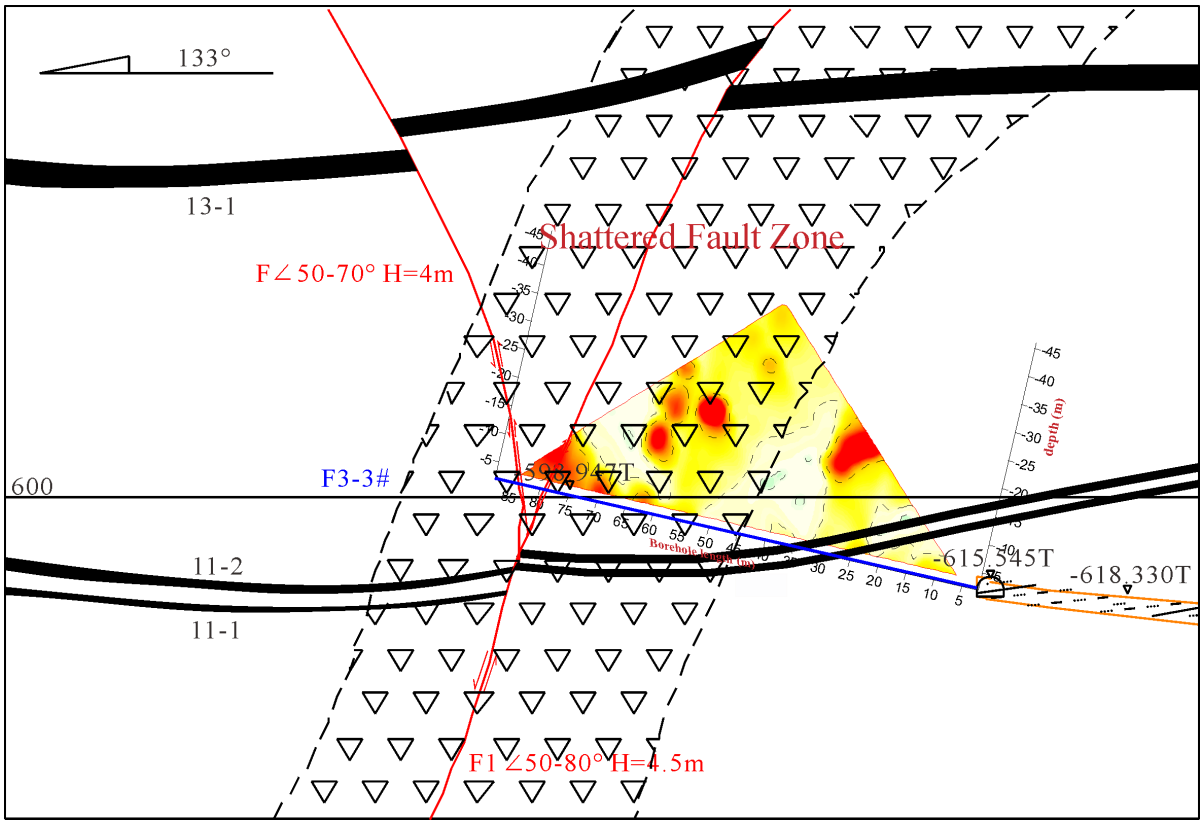
133°
13-1
Shattered Fault Zone
F∠50-70° H=4m
F3-3#
600
11-2
11-1
-615.545T
-618.330T
F1∠50-80° H=4.5m

(d)

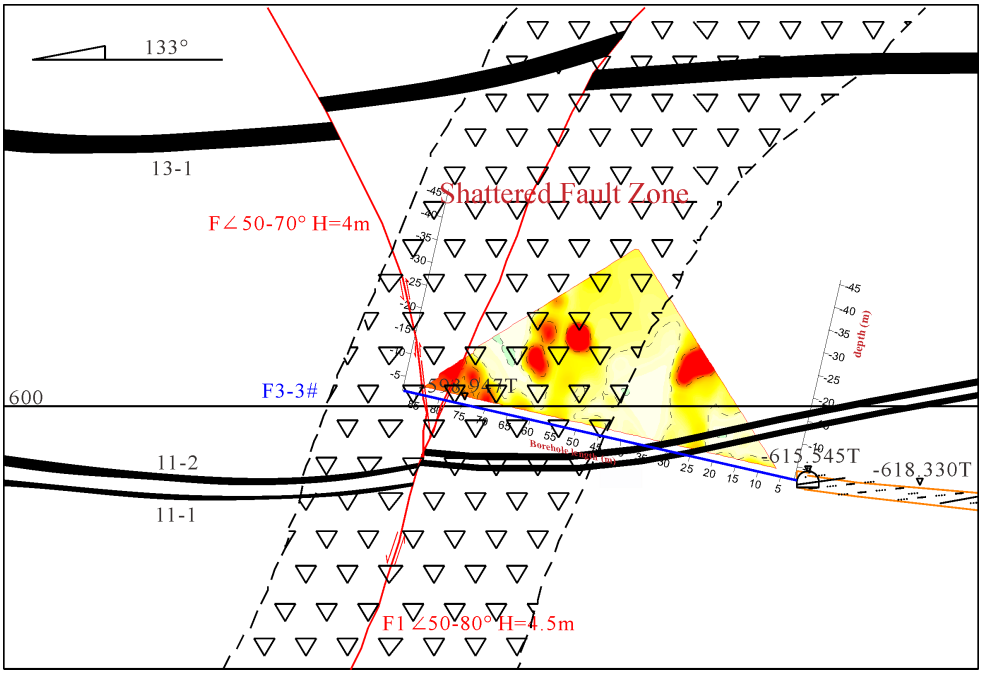

(e)

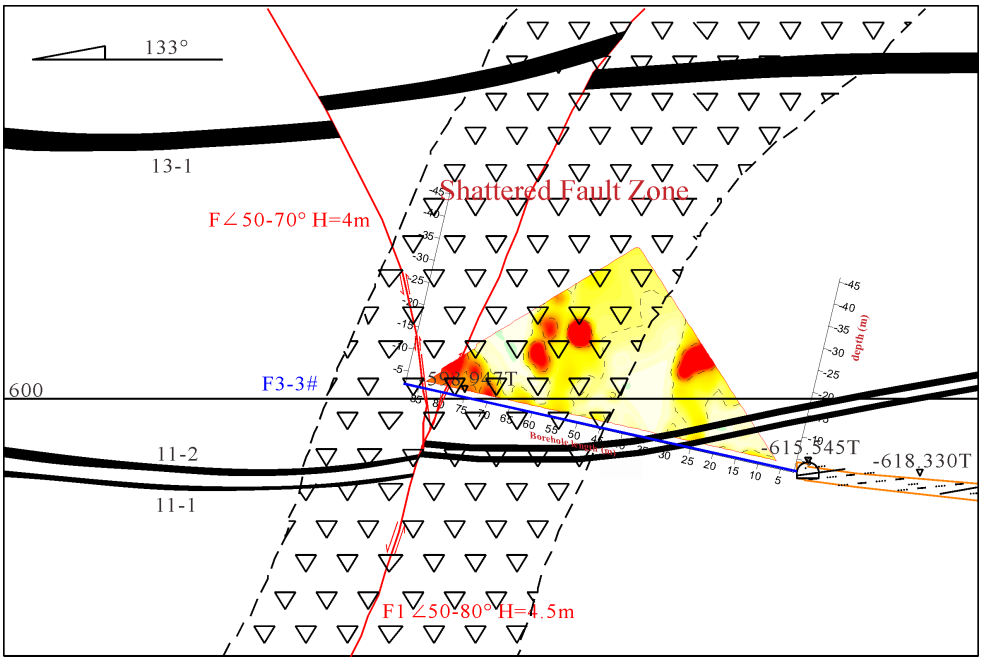

(f)

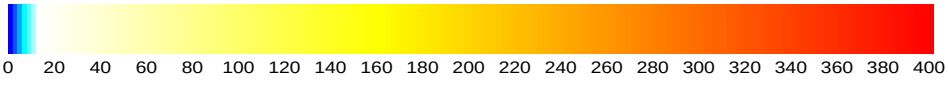

(Apparent resistivity Ω·m)

Figure 4. Apparent resistivity result of F3-3# borehole. (a) Figure of apparent resistivity of F3-3# borehole on 26 March 2020; (b) Figure of apparent resistivity of F3-3# borehole on 30 April 2020; (c) Figure of apparent resistivity of F3-3# borehole on 20 May 2020; (d) Figure of apparent resistivity of F3-3# borehole on 22 June 2020; (e) Figure of apparent resistivity of F3-3# borehole on 20 August 2020; (f) Figure of apparent resistivity of F3-3# borehole on 22 January 2021.

water-bearing capacity. The high value part of apparent resistivity should be attributable to the fault-fracture zone, which mainly came from the high resistivity characteristics after grout solidification. Figure 4(b) shows certain changes in apparent resistivity within the borehole, which were reflected by low resistivity regions at the top and middle parts of the borehole and an expansion of the high-resistivity region near the low-resistivity region. Our analysis indicated that rock strata in the section were normal sand and mudstone strata with fairly good integrity. Therefore, the rock strata in this section received less grouting slurry and had a generally small rock mass strength, making them highly susceptible to the influence of roadway excavation. Strain changes in surrounding rock amidst the excavation process also caused structural change in surrounding rock and may also lead to a certain level of fracture development, and the low-resistivity region should have been formed by the filling of small amounts of sand water following rapture development, which then affected the apparent resistivity value in the section. After the completion of roadway construction, as shown in Figure 4(c), the apparent resistivity value at centers of low-resistivity regions in the top and middle parts of the borehole declined further as roadway excavation continued in the fault zone till the completion of construction, but without significant expansion in scope. Our analysis indicates that fractures in rock strata of this section did not develop further, and changes in surrounding rock basically stopped, causing a suspension of rapture growth in surrounding rock. Only a small amount of fissure water continued to aggregate in developed rapture regions, which affected the apparent resistivity value of this section and caused a relatively low value. As strain in surrounding rock of the roadway rebalanced, the apparent resistivity value in the surrounding rock of the borehole basically recovered to the original value range, as shown in Figure 4(d).

In the meantime, as can be seen from the apparent resistivity results of F3-3# borehole spanning from August 20, 2020 to January 22, 2021, as shown in Figure 4(e), Figure 4(f), the distribution of apparent resistivity of the monitoring borehole exhibited a consistent pattern in nearly 8 months after the completion of roadway, indicating that the F1 fault-rapture zone and its surrounding rock were basically stabilized without showing significant disturbance effect.

As can be seen from the distribution of strain obtained from the BOTDR distributed optical fiber sensors and characteristics of resistivity changes in F3-3# monitoring borehole, as roadway excavation continued, the fault-fracture zone and its surrounding rock gradually show deformation and damage, causing the optical cable to undergo tensile and compressive changes and bending at relevant positions, and subsequently leading to corresponding changes in resistivity values. Based on the strain distribution characteristics of the optical cable and patterns of resistivity changes in F3-3# borehole, it can be inferred that the stability of the fault-fracture zone effectively increased after grouting reinforcement from ground surface and the degree of fault activation both before and after the roadway construction was relatively low.

6. Conclusions

Based on the monitoring of stability of surrounding rock of roadway excavated in complex geological conditions, the optical fiber and electrical methods are proposed to comprehensively evaluate the stability of surrounding rock in F1 fault passed through by roadway excavation and the effect of grouting. The following conclusions are drawn:

1) Utilizing integrated monitoring approaches of borehole optical fiber and resistivity methods helps accurately determine the stability of surrounding rock during roadway excavation. The integrated monitoring approach has advantages like good sensing performance and ability to satisfy monitoring requirements for surrounding rock in complex geological conditions.

2) After implementing grouting reinforcement from ground surface, the physical and mechanical properties of rock mass in F1 fault-fracture zone showed significant changes, as represented by high apparent resistivity and high compressive and tensile strengths, exhibiting significant differences from the lithology of normal strata.

3) Based on the strain distribution characteristics and patterns in the change of apparent resistivity responses of optical fiber and the geological profile of the borehole, it can be determined that after the construction of roadway excavation, the F1 fault experienced a relatively low degree of activation, indicating a good effect of grouting reinforcement from ground surface, and the strength of the rock mass in reinforced fault satisfies the requirement of safe production.

To conclude, using the integrated approach of borehole optical fiber and resistivity methods fulfills full-cycle dynamic monitoring of the stability of the fault-fracture zone and the effect of grouting reinforcement during roadway excavation, thereby offering a new testing approach for research of surrounding rock stability in roadway excavation.

Acknowledgements

The authors are grateful to National Natural Science Foundation of China (grant number 41877268) and the Graduate Innovation Fund Project of Anhui University of Science and Technology (No. 2020CX1001).

Conflicts of Interest

The authors declare no conflicts of interest regarding the publication of this paper.

References

[1] Li, L.J., Qian, M.G. and Li, S.G. (1996) Mechanism of Water-Inrush through Fault. *Journal of China Coal Society*, **21**, 119-123.

[2] Zhang, J.G. (2012) Advance Support Technology in Rock Roadways Excavation through Faults Fracture Zone. *Coal Technology*, **31**, 90-91.

[3] Shi, Z.Y., Li, H.W., Yu, H.Y., *et al.* (2015) Application and Practice on Fully Mecha-

nized Caving Face Passing through Fault. *China Coal*, **41**, 68-70, 73.

[4] Zou, Q.L. (2019) Reinforcement Technology of Fully Mechanized Working Face Passing through Fault Fracture Zone. *Shandong Coal Science and Technology*, No. 7, 75-76, 81.

[5] Zhang, Y. (2013) Application of Reinforcement by Pre-Grouting in Long Borehole for Mechanized Longwall Passing through Faults. *Journal of Anhui University of Science and Technology* (*Natural Science*), **33**, 63-68.

[6] Sun, B.Y., Zhang, P.S., Fu, M.R., *et al.* (2017) Fiber Optic Test and Results of Failure Law of Floor Strata in Coal Mining Site. *Journal of Hefei University of Technology* (*Natural Science*), **40**, 701-707.

[7] Zhang, P.S., Lu, H.F., Han, B.W., *et al.* (2019) Monitoring and Analysis of Deformation Characteristics of Fault Structure under Mining Condition. *Journal of Mining & Safety Engineering*, **36**, 351-356.

[8] Chai, J., OuYang, Y.B., Zhang, D.D., *et al.* (2020) Theoretical Analysis of the Mechanical Coupling between Rock and Optical Fiber for Distributed Sensing of Overlying Strata Deformation. *Journal of Mining and Strata Control Engineering*, **2**, 73-82.

[9] Zhang, D., Zhang, P.S., Shi, B., *et al.* (2015) Monitoring and Analysis of Overburden Deformation and Failure Using Distributed Fiber Optic Sensing. *Chinese Journal of Geotechnical Engineering*, **37**, 952-957.

[10] Sun, B.Y. (2018) Study on Strain and Geoelectric Response Characteristics and Test of Deformation and Failure of Surrounding Rock in Stope. Master's Thesis, Anhui University of Science and Technology, Huainan.

[11] Han, P. (2020) Forward Modeling and Inversion of the High-Density Resistivity Method in Detecting Karst Caves of Different Filling Types. *Geology and Exploration*, **56**, 1219-1225.

[12] Tan, L., Zhang, P.S. and Sun, B.Y. (2016) Resistivity Imaging Technology Applications in Hard Field Research. *Science Technology and Engineering*, **16**, 26-31.

[13] Sun, B.Y. and Zhang, P.S. (2021) Research Progress and Prospect of Surrounding Rock Deformation and Failure Monitoring in Stope Based DFOS. *Journal of Engineering Geology*, **29**, 985-1001.

[14] Zhang, P.S. and Sun, B.Y. (2020) Distribution Characteristics of the Advance Abutment Pressure in a Deep Stope. *Journal of Geophysics and Engineering*, **17**, 686-699. https://doi.org/10.1093/jge/gxaa022

[15] Zhang, P.S., Liu, S.D. and Wu, R.X. (2009) Dynamic Detection of Overburden Deformation and Failure in Mining Workface by 3D Resistivity Method. *Chinese Journal of Rock Mechanics and Engineering*, **28**, 1870-1875.

[16] Sun, B.Y., Zhang, P.S., Wu, R.X., *et al.* (2018) Dynamic Detection and Analysis of Overburden Deformation and Failure in a Mining Face Using Distributed Optical Fiber Sensing. *Journal of Geophysics and Engineering*, **15**, 2545-2555. https://doi.org/10.1088/1742-2140/aad1c6